

FSI Computation and Experimental Verification of Fluid Flow in Flexible Tubes

Dominik Šedivý¹, Simona Fialová¹, Roman Klas¹, Michal Kotek²

¹Brno University of Technology, Viktor Kaplan Department of Fluids Engineering, Technická 2896/2, 61669 Brno, Czech Republic, corresponding author email: fialova@fme.vutbr.cz

²Department of Physical Measurement, Technical University of Liberec, The Institute for Nanomaterials, Advanced Technology and Innovation, Studentska 1402/2 Liberec 1 461 17, Czech Republic

Presented paper is focused on the experimental and computational study of fluid flow in pipes with flexible walls. One possible real example of this phenomenon is the blood flow in arteries or their substitutes in the human body. The artery material itself should be understood as anisotropic and heterogeneous. Therefore, the experiment was carried out on the deforming tube, made of silicone (polydimethylsiloxane - PDMS). Obtained results and observed events were verified by numerical FSI simulations. Due to the large deformations occurring during loading of the tube, it was necessary to work with a dynamic mesh in the CFD part. Based on experimental testing of the tube material, a non-Hookean and Mooney-Rivlin material model were considered. Blood flowing in vessels is a heterogeneous liquid and exhibits non-Newtonian properties. In the real experimental stand has been somewhat simplified. Water, chosen as the liquid, belongs to the Newtonian liquids. The results show mainly comparisons of unsteady velocity profiles between the experiment and the numerical model.

Keywords: Fluid Structure Interaction, Particle Image Velocimetry, simulations, experimental verification, flexible tubes.

1. INTRODUCTION

Presented paper is focused on the study of fluid flow in pipes with flexible walls. One possible real example of this phenomenon is the blood flow in blood vessels (especially large arteries) in the human body or their substitutes in the form of artificial blood vessels or allotransplants or xenotransplants. Degenerative cardiovascular disease, accompanied by atherosclerotic manifestations in dilatory or obliterate form, leads to blood circulation disorders or aneurysms, which, in particularly large arteries such as the aorta, may cause their rupture and subsequent bleeding [1], [2]. Degenerative vascular disease is generally at the top of the causes of death. Therefore, it is necessary to address this problem from the engineering point of view, which takes into account the behavior of real vessels or bioinert polymers loaded by pulsating fluid flow, based on experiment and predictive mathematical-physical models.

Although the present time offers extensive possibilities in the field of numerical methods, it is not easy to realize a faithful simulation of fluid flow through a flexible tube in a fluid-structure interaction (FSI) task [3]. In most cases the results are limited to an experiment or to a numerical simulation without comparison. In works [4] and [5] were done experimental measurements with pulsatile flow and

straight elastic tube. Next step was experimental simulation of flow in curved elastic tube [6]. All these works were done without any numerical comparison. On the other side there are papers like [7] and [8], which solved flow in more complicated geometries only by numerical methods. Due to the very low fluid flows, the non-stationary nature of physical quantities, the size of the simulated area, and the sensitivity to boundary and initial conditions, the degree of fidelity of the results achieved by numerical simulation can be problematic. On the other hand, in the experiment it is practically impossible to achieve the same conditions as in the human body, nor is it possible to obtain all the necessary data in this way. The aim of the study was therefore primarily to compare the experimental part realized by particle image velocimetry (PIV) with numerical results of fluid-structure interaction (FSI) simulation, which in addition to prediction allows a relatively large degree of evaluation and data collection for further study and analysis.

2. EXPERIMENT

The artery material itself should be understood as anisotropic and heterogeneous. It exhibits large elastic deformations and is classified as so-called hyperelastic materials [9], which are characterized by non-linear

dependence between stress and strain. It is impossible to define average material properties of arteries. The properties depend on type of artery, gender, age and state of health [10]. Blood flowing in blood vessels is a heterogeneous liquid and exhibits non-Newtonian properties [11]. As it was mentioned, in the real experiment it is practically impossible to simulate the same conditions as in the human body, and therefore the experimental stand has been somewhat simplified (see Fig.1.). Water, chosen as the liquid, belongs to the Newtonian liquids. For the purposes of basic research, the gradual steps in selecting a more common fluid were deliberate with a view to defining the effects of individual components, materials and models so that the individual effects could be separated from each other and assessed well. For this reason, only flow in a straight unbranched tube was also addressed.

The deforming tube itself was made of silicone (polydimethylsiloxane - PDMS), which as subsequently considered hyperelastic and homogeneous [12], [13]. The experimental circuit was further composed from a diaphragm pump as a source of pulsating flow, a relatively rigid pipeline (relative to silicone), a vent valve, two pressure sensors (located in front of and behind the tube), and a high speed camera. In this case it was a 2D PIV, in which only one plane is being sensed.

To prevent tube oscillation, the tube was preloaded in the axial direction by 10 mm and fixed at both ends by clamps to simulate the fixed support. This also partially reduced unwanted deflection of the tube from the straight direction. Nevertheless, there was some slight deflection of the tube to the sides. The main properties of the experimental equipment are listed in Table 1. It is obvious that the frequency of diaphragm pump is very low. This is essential to make a decision if the material behavior is viscoelastic or not [12]. Since the frequency is low, the material was considered only as hyperelastic without any losses.

In the following Fig.2. shows the static pressure at the inlet and outlet of the tube and the mean cross-sectional velocity for one period. The measured point in the case of velocities of course corresponds to half the length of the experimental tube, see Table 1. It is apparent from the results that the velocity field varies considerably in spite of the relatively calm pressure course. This phenomenon is mainly caused by fluctuating pressure differential, which is not at first sight in Fig.2.

The effect of the elastic deformations of the tube on the velocity of the liquid is partly evident at the inlet and outlet of the tube, which of course cannot be studied by the experiment. It is very problematic to place a high-speed camera at the same time on the pressure sampling position for positional and optical reasons. Data from Fig.2. was then used to define boundary conditions for numerical simulation. The course of velocities for the next periods is shown in Fig.3. It is obvious from the time record of individual periods that the plot is not perfectly periodic. This is due to the inaccuracies of measurement and especially the characteristics of the experimental circuit, which is conceived as closed.

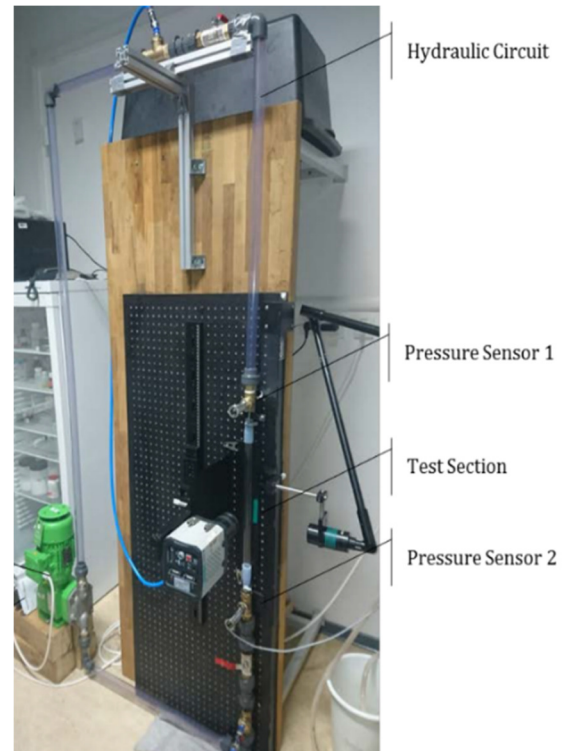


Fig.1. Experimental stand.

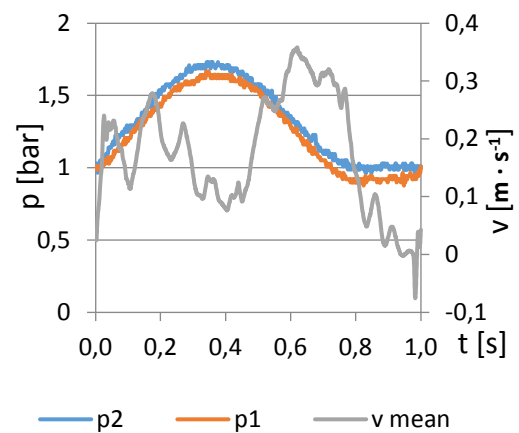


Fig.2. Experimental results for one period.

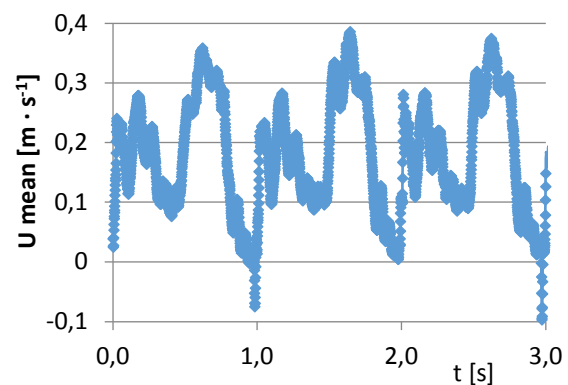


Fig.3. Mean axial velocity for 3 periods.

Table 1. Experimental stand properties.

Pipe properties	Length	Inner diameter	Wall thickness	Material
	500 mm	18.1 mm	2.2 mm	PDMS
Pump frequency	~ 1 Hz (0.968 Hz)			
Pressure sensors	Range	Accuracy	Sensors distance	Frequency
	0 – 2 bar	0.35 % max. range	630 mm	500 Hz
2D PIV	Sensing frequency of camera		Sensing position	
	1000 Hz		Middle of the pipe length	

3. NUMERICAL FSI SIMULATIONS

As mentioned in the introductory passage, the main means of verifying and inducing the events observed during the experiment were numerical FSI simulations. These simulations were performed in ANSYS Workbench 17.2, where System Coupling was used to bind finite element method (FEM - solid phase) and finite volume method (CFD - liquid phase) [14]. Stress-strain analysis utilized Transient Structural and fluid flow simulation was performed using ANSYS Fluent solver. The geometry corresponded to the experiment, but due to the time-consuming simulation, only a quarter of the tube was considered (see Fig.4. and Fig.5.). In other tests tested, it was verified that the data obtained for a quarter and the entire cross-section of the tube showed absolutely minimal deviations in the static pressure overpressure range. Under the vacuum resulting from the implementation of the closed experimental circuit, the internal cross-section of the solid tube cannot be reduced to a level less than the initial unloaded configuration. This results in deformation of the shape of the circular cross-section of the tube and consequent significant deflection of the tube from the direct direction due to additional stresses.

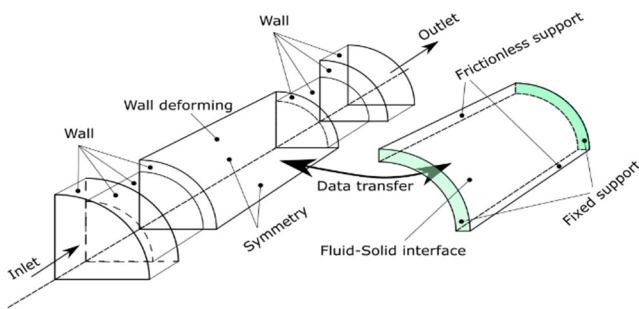


Fig.4. Scheme of fluid and structural domain geometries and boundary conditions.

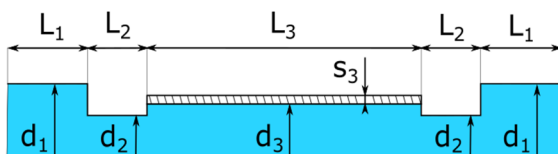


Fig.5. Dimensions of fluid domain.

Table 2. List of symbols.

A_r, A_{NH}, A_{MR}	[N ⁻¹ m ³]	Transform relation
C_1, C_2	[Pa]	Mooney-Rivlin material constants
d, d_1, d_2, d_3	[m]	Inner diameters of the simulated domain
E	[Pa]	Young modulus
f	[-]	Darcy friction factor
g	[m s ⁻²]	Gravity acceleration
G	[Pa]	Initial shear modulus
\bar{I}_{1C}	[-]	First invariant of the right Cauchy-Green deformation tensor
$\bar{I}_{1B}, \bar{I}_{2B}$	[-]	First and second invariant of the right Cauchy-Green deformation tensor
K	[Pa]	Bulk modulus
L_1, L_2, L_3	[m]	Length parts of simulated domain
p, p_1, p_2	[Pa] [bar]	Static pressure and absolute static pressures for domain inlet and outlet
$r_{31} = d_3/2, r_{32}$	[m]	Variable inner and outer radius of the tube
r_{310}, r_{320}	[m]	Starting inner and outer radius of the tube
s_3	[m]	Wall thickness of tested tube
t	[s]	Time
U	[m s ⁻¹]	Experimental velocity value in the tube
v	[m s ⁻¹]	Flow velocity in the tube
W	[Pa]	Strain energy density
x	[m]	x-coordinate, axis of the tube
μ	[Pa s]	Dynamic viscosity-liquid
ν	[-]	Poisson's ratio
ρ, ρ_F	[kg m ⁻³]	Tube and liquid density

Table 3. Range of the calculated domain.

$L_1 = 25$ mm	$d_1 = 25$ mm	$s_3 = 2.2$ mm
$L_2 = 40$ mm	$d_2 = 15$ mm	
$L_3 = 500$ mm	$d_3 = 15$ mm	

Table 4. Description of numerical model.

Simulation	FEM	CFD
Material	neo-Hookean	water
Material constants	$\rho = 1210 \text{ kg.m}^{-3}$ $E = 1.9 \text{ MPa}$ $\nu = 0.5$ $G = 0.633 \text{ MPa}$	$\rho_F = 998.2 \text{ kg.m}^{-3}$ $\mu = 0.001 \text{ Pa.s}$
Nr. of cells	10 000	249 000
Type of elements	quadratic, Hex 20	linear, Hex 8
Max. skewness	0.03	0.50
Max. Aspect ratio	2.81	3.92
Boundary conditions	Frictionless, Fixed, Fluid solid interface	Velocity inlet (pressure inlet) Pressure outlet
Damping Control and dynamic mesh update method	Numerical Damping: 0.1	Diffusivity Based on Cell Volume Diffusion Parameter: 0
Solution Stabilization	-	Coefficient-based Scale Factor: 0.002
Calculation mode	Unsteady, time step = 0.005 s, incompressible and laminar flow, incompressible solid	
Reynolds number in the middle of the tube	~ 0 - 8000	

This phenomenon can be countered as in the experiment by preloading the tube. In the case of hyperelastic Neo-Hookean materials, the prestressing alone does not have a significant effect on the magnitude of the radial deformations of the tube, if a purely circular cross-section is considered, the same value of axial stresses on the inner and outer radius of the tube and the fixed tube length. The calculation time of the bound task (System Coupling mode) is at the limit of acceptability even with such a simple task due to possible testing and verification of the results. Simulations were done on computer station with following hardware: AMD Ryzen 5 2600x Six-Core Processor, RAM 32 GB. One period of simulation (200 coupling steps) took about 20 hours of computing time. The fact that the full tube considered would be, like its quarter of a purely circular cross section, speaks to the reduction of the tube to a quarter. However, the actual tube exhibits some variations in circularity and wall thickness. In the following Table 2. to Table 4. are used markings, computer domain dimensions and numerical model settings. Sensitivity analysis is a part of all numerical simulations. If experimental data exists, the main criterion is the match of the numerical simulation result with the experiment. In this particular case, the number of solid and liquid phase computational cells in the radial and axial

direction was therefore monitored with respect to their minimum number.

Due to the large deformations occurring during loading of the tube, it was necessary to work with a dynamic mesh in the CFD part of the task. Therefore, Dynamic Mesh Update Methods in Diffusion-Based Smoothing were chosen in the deforming regions, which seemed to be the most suitable of the available options, see Table 4. All zones of the fluid domain except for the liquid-elastic wall interface (wall deforming, see Fig.4.) were then defined as deforming. However, the position of these zones has been fixed by coordinates and vectors because the position of these entities is in fact constant or fixed. The wall deforming interface was subject to the System Coupling setting within which data are shared and transferred between the structural and fluid solver. Due to the problems with the convergence of the simulation, the Solution Stabilization was also used, see Table 4. The setting of the stabilization coefficient can significantly influence the simulation, e.g. in the vacuum area.

The liquid in the CFD simulation made up of pure water did not contain other particles that were, by nature, part of the experiment. However, the concentration of these particles must be less than 2 % at a very low level with a density close to water. Therefore, these particles have no significant effect on the results obtained. The tube flow regime was considered laminar. This fact, which at first glance contradicts a meaningful conception of the task, because in the centre of the tube reaches Re value up to 8000, has its reason. In the follow-up work should be tested liquid, which falls into the category of non-Newtonian similar to blood. However, the turbulent behavior of non-Newtonian fluids is not yet sufficiently described [14], [15], [16]. From this point of view, it is more certain to consider only laminar flow, even with regard to the experience gained for the follow-up work. The second reason in using the laminar flow regime is the boundary conditions. It is known that it is necessary either to import the input velocity profile (in this case unsteady) into CFD solver, but this is not known due to the location of the pressure sampling, or to extend the area by a free section of the pipeline where the corresponding velocity profile is generated. However, the lengthening of the computational domain brings a considerable distortion of the results achieved, since the computational domain itself is relatively short. In the input cross section defined by the diameter d_1 in Fig.5., the Reynolds number is even greater than half the length of the tube. This is one reason why the expected unsteady turbulent velocity profile has been replaced by a non-stationary piston profile that corresponds to the velocity inlet condition with a constant velocity distribution across the cross-section.

In addition to the definition of boundary conditions, the setting of the structural solver consists in prescribing a suitable hyperelastic material. Based on experimental testing of the tube material, a non-Hookean (1) and Mooney -Rivlin (2) material model was considered to be the most suitable neo-Hookean with regard to the less problematic convergence of the problem.

$$W = \frac{G}{2}(\bar{I}_{1C} - 3) \quad (1)$$

$$W = C_1(\bar{I}_{1B} - 3) + C_2(\bar{I}_{2B} - 3) \quad (2)$$

The tensile modulus of PDSM of material E was determined by a uniaxial tensile test and its properties are listed in Table 4. In terms of fidelity of numerical simulation, the choice of boundary conditions is essential. The input and output values of static pressures are known from the experiment, see Fig.2., but which do not represent a complete specification of the boundary conditions of the fluidic part of the simulation. A common combination of boundary conditions in a CFD simulation is a combination of velocity and static pressure conditions, or a combination of two pressure conditions. In the latter case, however, one of the pressures shall be the total pressure containing the dynamic component. The dynamic pressure component is relatively small and is often neglected in some applications. However, due to the relatively small dimensions of the tube, dynamic pressure is important. In the case of an absolutely rigid tube, it would of course be possible to use the magnitude of the mean velocities obtained by the 2D PIV method at half the tube length to determine the dynamic component. However, in the case of a flexible tube, the dynamic pressure at the inlet or outlet to the computing area will differ considerably compared to the dynamic pressure at half the length of the tube. Therefore, boundary conditions are required in connection with Fig.2.

There are two ways to deal with the problem. The first variant assumes that the tube is halved, the mean speed of Fig.2. at the outlet of the tube while using the experimentally determined static pressure at the inlet of the tube. It is actually a combination of speed and static pressure conditions. After performing this FSI simulation, the approximate size of the dynamic pressure component at the inlet of the tube can be gradually determined. The basic criterion for the correctness of such a procedure, but not the only one, is, of course, the FSI simulation of the original tube with the pressure output condition corresponding to the experiment, while maintaining the mean velocity at the center of the tube, which also corresponds to the experiment. The second way to define the dynamic component of the inlet pressure is a one-dimensional FSI simulation representing a combination of a fluid equation of motion (3), a continuity equation (4) and at least a simple solid phase equation of motion (5) assuming a fixed length tube. The density of the tube material is close to water, see Table 4. and therefore it makes no sense to consider its inertial effects. The question of the viscous behavior of the material has already been answered in relation to the frequency of pressure pulses in the experimental circuit. It should further be noted that although in the relationship (4) there is a modulus of liquid compressibility K , the liquid is nevertheless understood to be incompressible. However, the convergence of the 1D model is more favorable with this setting. The equation of motion of the tube (5) can easily be extended by 1D models with neo-Hookean material (6) or Mooney-Rivlin can be tested with two parametric material models (7) with constants $C_1 = 292308$ Pa and $C_2 = 24359$ Pa.

$$\frac{\partial v}{\partial t} + v \frac{\partial v}{\partial x} = g - \frac{1}{\rho_F} \frac{\partial p}{\partial x} - \frac{f}{2r_{31}} \frac{v|v|}{2} \quad (3)$$

$$\frac{\partial p}{\partial t} = \frac{-K \frac{\partial v}{\partial x}}{1 + \frac{2KA_r}{r_{31}}} - v \frac{\partial p}{\partial x} \quad (4)$$

$$\frac{\partial r_{31}}{\partial t} = A_r \frac{\partial p}{\partial t} \quad (5)$$

$$A_r = A_{NH} = \frac{1}{2r_{31}G \left(\frac{r_{310}^2}{r_{31}^4} - \frac{r_{320}^2}{r_{32}^4} \right)} \quad (6)$$

$$A_r = A_{MR} = \frac{1}{4r_{31} \left[C_1 \left(\frac{r_{310}^2}{r_{31}^4} - \frac{r_{320}^2}{r_{32}^4} \right) + C_2 \left(\frac{1}{r_{310}^2} - \frac{1}{r_{320}^2} \right) \right]} \quad (7)$$

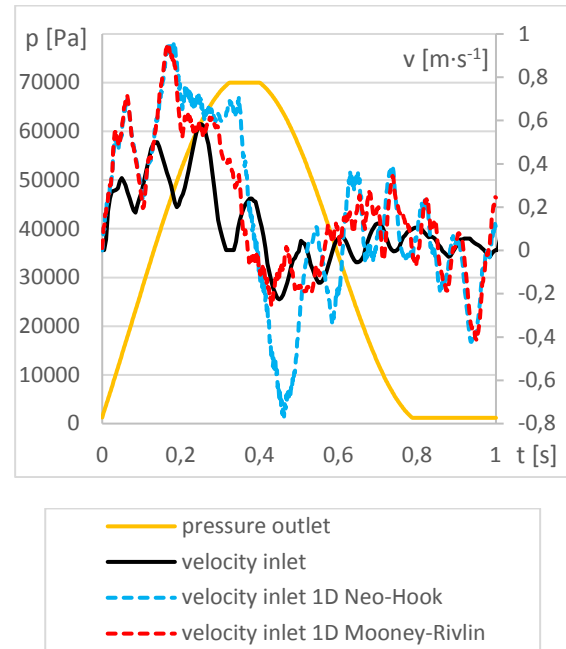


Fig.6. Boundary conditions for CFD and 1D simulations of the inlet velocity.

Both ways were used to realize the final FSI simulation of the test tube. In connection with the above, it is necessary to mention one more fact, which is based on the possibilities of the experiment. In Table 1., the accuracy of pressure transducers at 0.35 % of their maximum measurable range of 2 bar, i.e. 700 Pa, is mentioned. The absolute pressure sizes are relatively large, but the pressure differential of the static pressures between the inlet and the outlet of the tube takes substantially smaller values. The tube itself is only 500 mm long, so the pressure drop is minimal and the hydrostatic pressure is also small. Even when using another type of encoder with a higher accuracy class, a measurement error for a similar task cannot simply be neglected. It is therefore advisable to eliminate undesired pressure inaccuracies or at least the static outlet pressure of Fig.2. is a simpler curve, see Fig.6. The course of static pressure was therefore replaced by

the polynomial of the 6th degree and in the steady-state areas by a straight line. In Fig.6., the results of 1D FSI simulations obtained through relationships (3) to (7) for the neo-Hookean and Mooney-Rivlin material models are also recorded. It seems that 1D simulations are particularly suitable for checking the results obtained or as a starting point for refining boundary conditions. Better match of 1D Mooney-Rivlin material model over 1D neo-Hookean material in Fig.6. compared to the final form of the inlet velocity inlet boundary condition in ANSYS FSI simulation is not critical. The reason is of course the term in the denominator of the relation (7), which stands at the constant C_2 , and which is itself a constant. It is known that the sum of C_1 and C_2 corresponds to $G / 2$ if $\nu = 0.5$ (Table 4.). The larger amplitude magnitude of the 1D neo-Hookean model in Fig.6. is due to the nature of the numerical 1D model and the input boundary conditions, which are in parts by continuous functions, defined by the measurement interval, to which this model can respond worse than the Mooney-Rivlin model. Of course, it is ideal to fit boundary conditions with one continuous function, if possible. However, by default, purely experimental data was used in 1D simulations.

4. RESULTS

As it was mentioned before, one of the FSI simulation accuracy criteria was the match of mean velocities at half the length of the tube compared to the experimental data. The comparison is shown in Fig.7.

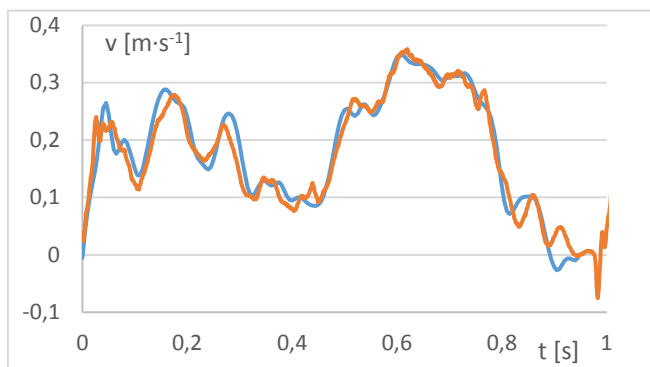


Fig.7. Comparison of the average velocity values during one period.

The waveforms of both curves are fairly consistent, but it is evident that the numerical calculation did not affect all the dynamics of the experimental data. This can be caused by different size of time step in FSI simulation, but also by different tasks. We are not able to cover all the characteristics of the experimental track in the simulation. The size of the time step in FSI simulation, in turn, is related to the total computation time, see Table 1. and Table 4., which, if the time scale is the same as in the experiment, would grow five

times. Equally important criteria for simulation fidelity are the time sequences of velocity profiles set at half the tube length. If we were to consider a real application in the form of blood flow in arteries, we would get a more or less faithful picture of the dynamics of blood circulation in the affected area. For example, it is no longer difficult to analyze the relevant tube stresses or arteries in the FSI simulation. However, since experimental data is missing for obvious reasons, the corresponding stresses will not be plotted. Indeed, stress analysis of rotationally symmetric bodies is well described in literature [5], [17], [18]. Other works [3], [7], [19], which were carried out at this topic, show that the link between the static pressure in the tube and the actual or simulated deformation of the tube is less prone to possible inaccuracies than is the case with purely hydraulic parameters. By this is meant the coupling between the static pressure and the corresponding flow velocity, which can be faithfully simulated in the flexible tube substantially more difficult. Therefore, the following figures (Fig.8. to Fig.24.) show mainly comparisons of velocity profiles between the experiment and the numerical model. The curve corresponding to the FSI simulation only extends to half the profile as it corresponds to a quarter of the simulated tube. The actual width of the planar experimental velocity profile may vary because the hose, in contrast to the simulation, swung sideways while the high-speed camera position was stationary.

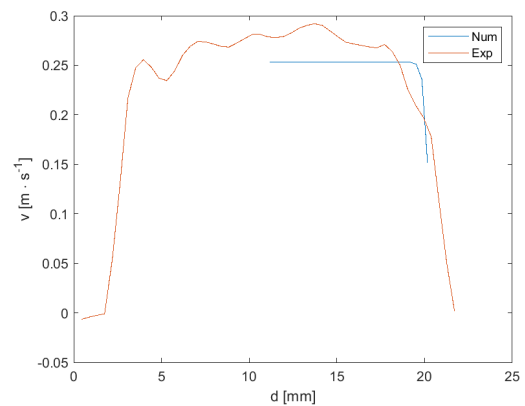


Fig.8. t = 0.05 s.

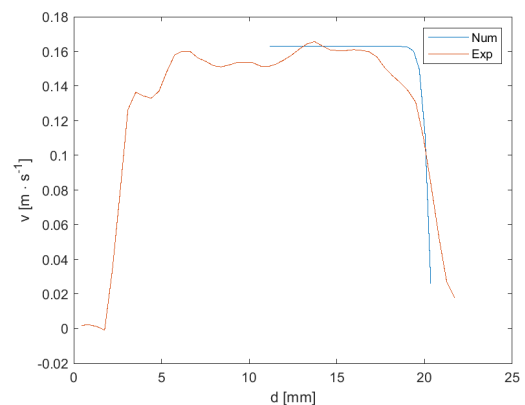


Fig.9. t = 0.1 s.

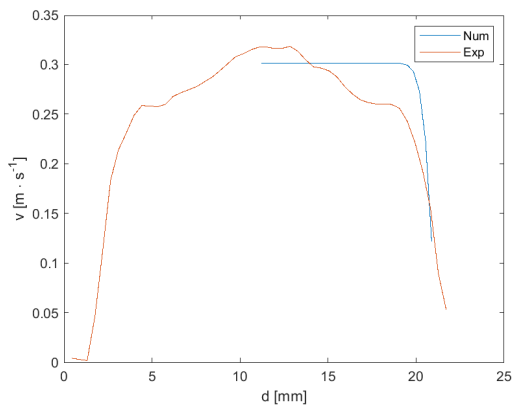


Fig.10. $t = 0.15$ s.

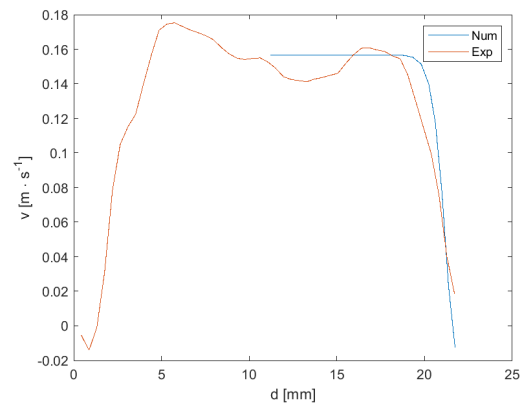


Fig.14. $t = 0.35$ s.

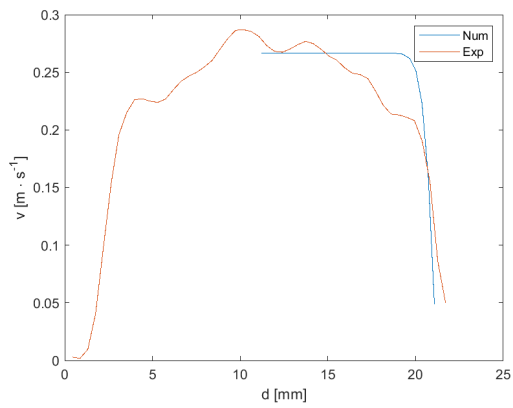


Fig.11. $t = 0.2$ s.

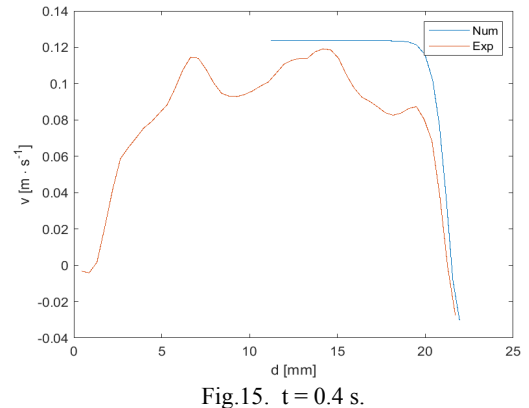


Fig.15. $t = 0.4$ s.

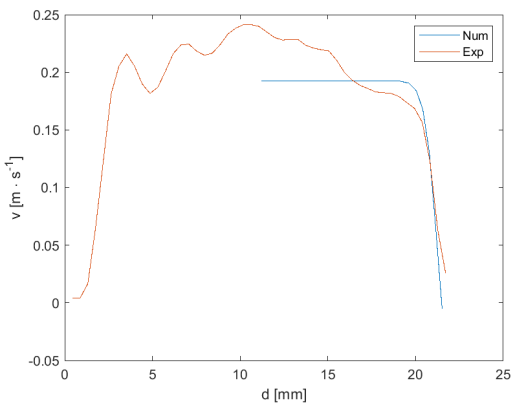


Fig.12. $t = 0.25$ s.

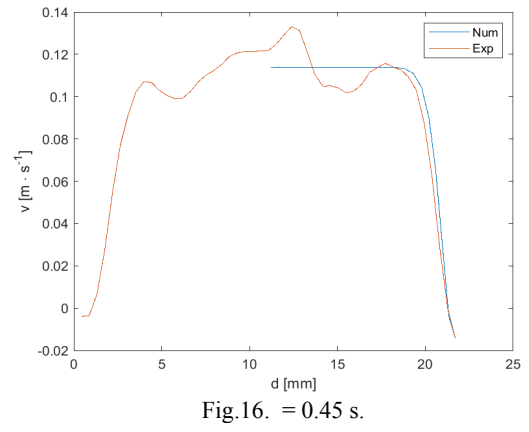


Fig.16. $t = 0.45$ s.

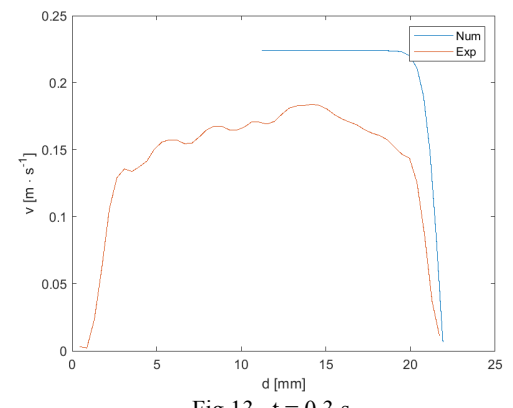


Fig.13. $t = 0.3$ s.

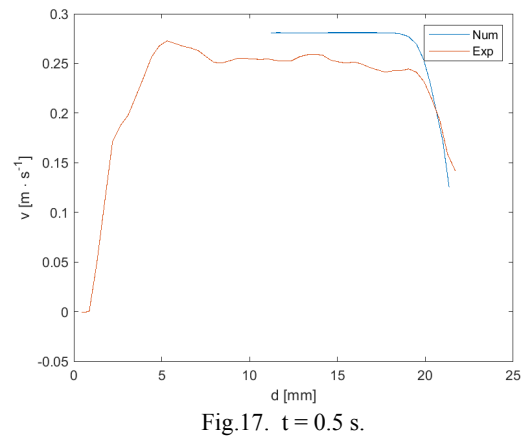


Fig.17. $t = 0.5$ s.

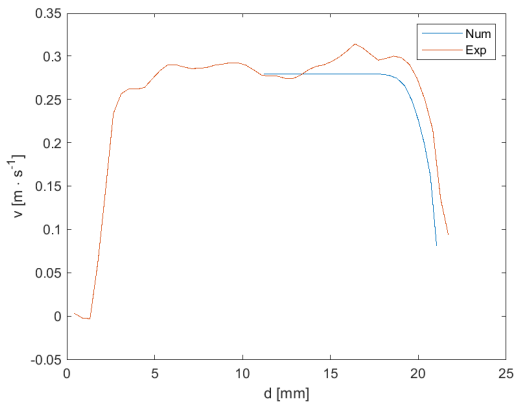


Fig.18. $t = 0.55$ s.

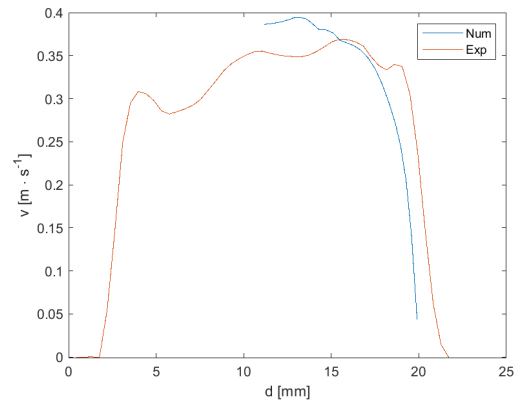


Fig.22. $t = 0.75$ s.

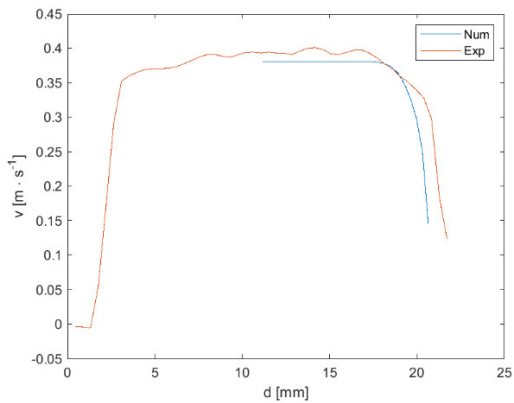


Fig.19. $t = 0.6$ s.

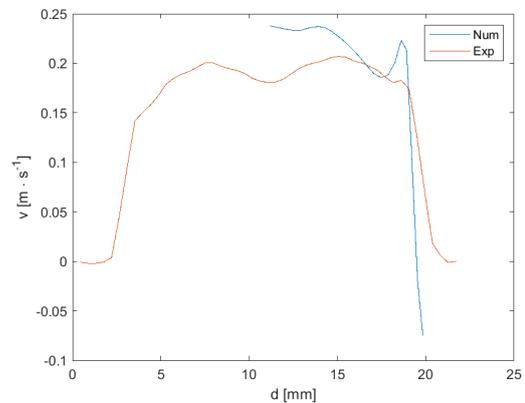


Fig.23. $t = 0.8$ s.

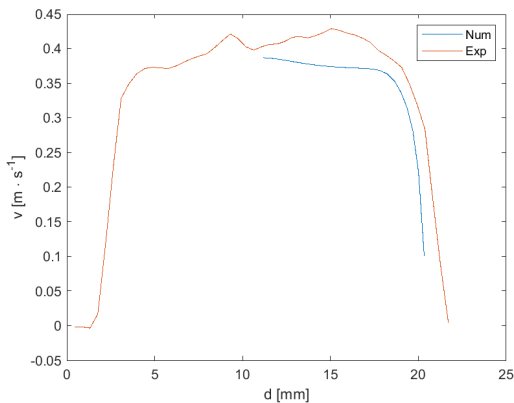


Fig.20. $t = 0.65$ s.

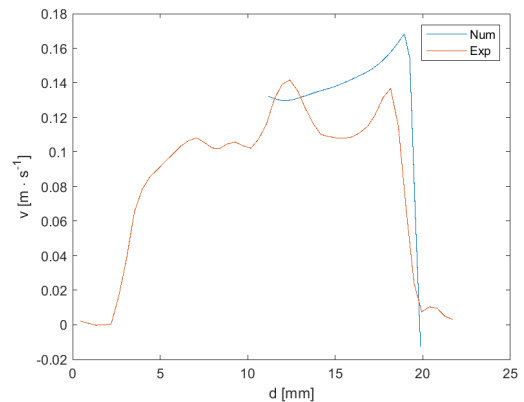


Fig.24. $t = 0.85$ s.

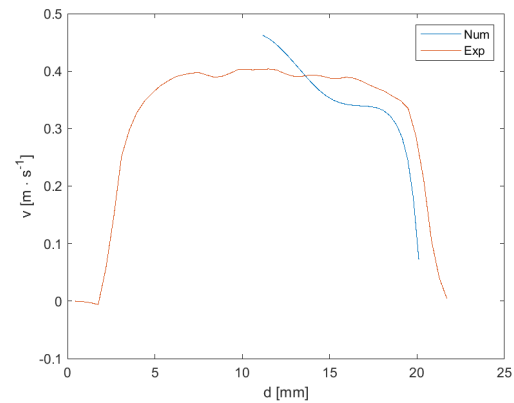


Fig.21. $t = 0.7$ s.

Obviously, the experimental velocity profiles exhibit a greater degree of instability and asymmetry due to the size of the time step and the continuous operation of the pump, which pulsates constantly vibrates the tube regardless of the theoretical beginning and end of the simulated period. It is also known that any such task depends greatly on the initialization conditions. In principle, however, in the first half of the simulated period, the speed profiles obtained through the FSI simulation in shape correspond quite well to the experiment. In the second part of the tested period, the asymmetry of the velocity profile further increases and the deviation between the experimental data and the numerical simulation increases. It can be further noted that if we assume

a symmetric velocity profile at the beginning of the simulated period (Fig.8. to Fig.11.), this symmetry is progressively disturbed during inflation of the hose due to pressure build-up in the system. The situation worsens when the static pressure reaches its maximum and the tube begins to shrink, which takes place in the second half of the period examined. For this, it is necessary to consider a slightly variable wall thickness of the actual tube, which leads to the formation of ovals and uneven deformation of the originally almost circular cross-section. In Table 3. it is stated that the thickness of the tube is relatively thin, corresponding to approximately 2.2 mm. Changes in thickness uniformity at the level of five to ten hundredths of millimeters will significantly affect the size of the radial deformations of the tube. The worst situation then occurs at the very end of the simulated period, when part of the tube gets under vacuum (see Fig.2.) and the velocity profile shows deviations from the profile simulated in size and shape. As mentioned previously, during the vacuum mode, the tube tends to deviate from the straight direction.

5. CONCLUSION

Although the tested domain is relatively simply shaped, FSI simulation of a cylindrical tube presents a number of problems with respect to the fidelity of the characteristic values of the flow field in the tube. We could consider and then simulate a branched tube similar or identical to the actual bloodstream, but such a problem has two weak points. The first is the true value of the experiment and the second is the fidelity of the FSI simulation. Both of these shortcomings are largely based on the relevance of boundary conditions and the fidelity of the experimental model, real and virtual.

The experiment described in this work most closely approximates the simulation of blood flow through large vessels with a high elastin content. The task of the large vessels is, among other things, to convert the pulse flow into a continuous flow. From this point of view, the experimentally measured flow in the tube, determined at half its length and described by the mean velocity of the cross-section, can be considered as acceptable.

In the experimental part of the work, it would be worth considering the implementation of an open hydraulic circuit, which would limit the effect of timing of the suction and discharge valves of the diaphragm pump. Thus, it would be possible to improve the compliance of the non-stationary course of physical quantities in individual periods and to reduce the vacuum area. Regarding the boundary conditions and thus the position of the measurement sites, reconfiguration of the experimental stand after the experimental data from the static pressure transducers could be useful. It has been said that it is relatively problematic to determine both static pressures and the character of an unsteady velocity field at the same measured position. Therefore, changing the pressure tapping point to the position of the high-speed camera seems to be an advantageous way, while maintaining the required optical conditions. Although it is still not possible to link the static pressure magnitudes to the corresponding velocity profile or velocity profile at the inlet of the tube and at half its length at one time, this would be beneficial as a guide to further adjusting the boundary

conditions. Of course, two high-speed cameras supplemented by a pressure sensor would be optimal. In connection with the sensing frequency of non-stationary static pressures and the choice of pressure transducers, we can certainly recommend work dealing with the dependence of the sensing frequency on the magnitude of the measured pressure amplitude with regard to its decrease due to damping.

In the field of FSI simulations implemented using commercial software ANSYS with CFD solver ANSYS Fluent, besides the mentioned boundary conditions, the so-called solution stabilization seems to be an important option. The size of the Scale Factor with the coefficient-based method chosen can significantly affect the simulated current field and unfortunately no clear opinion can be given with respect to its size. The value of the simulations was 0.002. As the value of this factor increased, the response of the change in velocity field to the change in static pressure in the system decreased.

The question of boundary conditions was already mentioned in connection with the evaluation of the experiment. For further determination in terms of simulations, there is no choice but to use the division of the tube into smaller units so that it is possible to use the experimentally determined velocity field at a particular location of the tube and make it a boundary condition. The combination of velocity and pressure conditions on the shortened tube eventually allows the necessary amount of dynamic pressure in the tube to arrive at the position of the pressure sensor. The disadvantage of such an approach is, of course, the time consuming, which is generally associated with FSI simulations.

Auxiliary one-dimensional FSI simulations are able to qualitatively capture the basic trend of mean velocities in the cross-section at the tube entry, but the error in the determination of mean velocity appeared quite significant. A disadvantage is also the nature of the tube material itself with respect to the frequency of pressure pulsations. Purely elastic, more precisely, hyperelastic tube behavior combined with experimental data yields more noticeable variations in mean velocity amplitude in 1D FSI simulations. Of course, internal damping can be introduced into one-dimensional models, but will result in unwanted attenuation of some frequencies that does not correspond to reality. In this context, the two-parameter Mooney-Rivlin material model appears to be more favorable than the neo-Hookean, which in 1D yields better results with respect to the concept of the relationship between radial deformation of the tube wall and the internal pressure in the tube. Considering the continuous functions of the input and initial conditions, the differences between the neo-Hookean and the two-parameter Mooney-Rivlin material model of the same tube in 1D FSI simulations would be small. By this is meant in particular the magnitude of the radial deformations of the tube and the velocity in the center of the tube. However, radial deformations of the tube are not part of the presented work. The estimation of the input mean velocity in the cross-section of the tube by 1D FSI simulations can then serve as a starting value for the subsequent refinement of the boundary condition, or as a control of the FSI simulation of the shortened tube, which uses the basic data

experimental mean values of cross-sectional velocities, e.g., half the length of the tube, and static pressure at the inlet of the tube.

The main criteria for evaluating the success of 3D FSI simulation were the mean velocity in the tube cross-section and the individual experimentally determined velocity profiles. Conformity of velocity profiles within the measured period may, in subsequent applications, indicate fidelity in the description of the blood system hemodynamics. Probably the biggest problem in the evaluation of experimental velocity profiles is the greater or lesser lateral deflection of the tube depending on the load on the tube wall. Thus, the stationary velocity camera is prevented from symmetrically sensing the velocity profile over the entire cross-section of the tube. As a result, information about the exact position of the inner walls of the tube is lost and the width of the planar experimental velocity profile differs slightly compared to the actual size of the inner diameter of the tube.

Comparison of velocity profiles from FSI simulations compared to experimental data can be evaluated as a match of velocity profile and maximum achieved velocities relatively good in the first half of the measured period during which the tube is inflated. At the same time, the symmetry of velocity distribution in the profile is gradually reduced with respect to the intended axis of the tube. Of course, this does not mean that the tube is deflected sideways. The velocity profile becomes increasingly unsymmetrical in the second part of the measured period when the tube is shrinking again, with the worst situation in this respect occurring in the vacuum area.

FSI simulation of a full cross section tube only partially solves this problem because lateral deflection is typical only for that vacuum area of the simulation. The geometry considered for the purposes of numerical simulations also assumes a constant wall thickness and a completely circular cross-sectional shape of the tube. In the case of a real tube neither of these two facts applies completely. The deviations are small in the order of hundredths and tenths of a millimeter, but they influence the stress and deformation of the tube. In a way, it is expected that CFD or FEM simulations based on symmetric geometric and boundary conditions will offer more symmetry than the experimental observation of a deforming tube almost in free space. This applies to the simulated full cross-section of the tube and its quarter except the already mentioned vacuum area. The FSI simulation of a full tube is significantly more sensitive to the convergence and stability of the solution in the vacuum area, for example because of the tube deflection from the straight direction. In this context, however, it should be added that there is no significant time-dependent movement to the sides of the blood vessels for obvious reasons.

The last neglected fact is the flow regime. It was stated that due to the lack of a description of the turbulent behavior of non-Newtonian fluids in the existing literature, the flow regime was considered laminar. If a different shear stress distribution in the tube cross-section and a different flow pattern near the deforming tube wall are considered in the follow-up works, this may result in some asymmetries in

velocity profiles in the full tube simulations during the inflation and contraction process. However, it is not yet possible to assess in advance whether this asymmetry will be predominantly of numerical or hydraulic origin.

ACKNOWLEDGEMENT

This paper has been supported by projects "Computer Simulations for Effective Low-Emission Energy Engineering" funded as project No. CZ.02.1.01/0.0/0.0/16_026/0008392 by Operational Programme Research, Development and Education, Priority axis 1: Strengthening capacity for high-quality research and "Interaction of heterogeneous liquid with flexible wall" funded as project No. GA101/17-19444S by Grant Agency of Czech Republic.

REFERENCES

- [1] Kinoshita, M., Yokote, K., Arai, H. et al. (2018). Japan Atherosclerosis Society (JAS) guidelines for prevention of atherosclerotic cardiovascular diseases 2017. *Journal of Atherosclerosis and Thrombosis*, 25 (9), 846-984.
- [2] Kannel, W.B. (1998). Overview of atherosclerosis. *Clinical Therapeutics*, 20 (suppl. 2), B2-B17.
- [3] Samaee, M., Tafazzoli-Shadpour, M., Alavi, H. (2017). Coupling of shear-circumferential stress pulses investigation through stress phase angle in FSI models of stenotic artery using experimental data. *Medical & Biological Engineering & Computing*, 55, 1147-1162.
- [4] Burgmann, S., Grosse, S., Schroder, W., Roggenkamp, J., Jansen, S., Gräf, F., Büsen, M. (2009). A refractive index-matched facility for fluid-structure interaction studies of pulsatile and oscillating flow in elastic vessels of adjustable compliance. *Experiments in Fluids*, 47 (4-5), 865-881.
- [5] Pielhop, K., Klaas, M., Schroder, W. (2015). Experimental analysis of the fluid-structure interaction in finite-length straight elastic vessels. *European Journal of Mechanics – B / Fluids*, 50, 71-88.
- [6] Pielhop, K., Schmidt, C., Zholtovski, S., Klaas, M., Schröder, W. (2014). Experimental investigation of the fluid-structure interaction in an elastic 180° curved vessel at laminar oscillating flow. *Experiments in Fluids*, 55 (10), 13.
- [7] Khader, S.M.A., Ayachit, A., Pai, B.R., Rao, V.R.K., Kamath, S.G. (2012). FSI simulation of common carotid under normal and high blood pressures. *Advances in Mechanical Engineering*, 2012, art. ID 140579.
- [8] Reymond, P., Crosetto, P., Deparis, S., Quarteroni, A., Stergiopoulos, N. (2013). Physiological simulation of blood flow in the aorta: Comparison of hemodynamic indices as predicted by 3-D FSI, 3-D rigid wall and 1-D models. *Medical Engineering & Physics*, 35 (6), 784-791.
- [9] Bergström, J. (2015). Elasticity / Hyperelasticity. In *Mechanics of Solid Polymers: Theory and Computational Modeling*. Elsevier, 209-307.

- [10] Riley, W.A., Barnes, R.W., Evans, G.W., Burke, G.L. (1992). Ultrasonic measurements of the elastic modulus of the common carotid artery: The Atherosclerosis Risk in Communities (ARIC) study. *Stroke*, 23, 952-956.
- [11] Robertson, A.M., Sequeira, A., Owens, R.G. (2009). Rheological models for blood. In *Cardiovascular Mathematics : Modeling and Simulation of the Circulatory System*. Springer, Vol. 1, 211-241.
- [12] Placet, V., Delobelle, P. (2015). Mechanical properties of bulk polydimethylsiloxane for microfluidics over a large range of frequencies and aging times. *Journal of Micromechanics and Microengineering*, 25 (3).
- [13] Kim, T.K., Kim, J.K., Jeong, O.C. (2011). Measurement of nonlinear mechanical properties of PDMS elastomer. *Microelectronic Engineering*, 88 (8), 1982-1985.
- [14] ANSYS, Inc. ANSYS Documentation 17.2.
- [15] Dodge, D.W., Metzner, A.B. (1959). Turbulent flow of non-Newtonian systems. *AIChE Journal*, 5 (2), 189-204.
- [16] Litvinov, W.G. (2011). Model for laminar and turbulent flows of viscous and nonlinear viscous non-Newtonian fluids. *Journal of Mathematical Physics*, 52 (5), 053102.
- [17] Klas, R., Fialová, S. (2019). Pulse flow of liquid in flexible tube. In *EPJ Web of Conferences*, 213, 02041.
- [18] Šedivý, D., Burša, J., Fialová, S. (2019). Experimental and numerical investigation of flow field in flexible tube. In *IOP Conference Series: Earth and Environmental Science*, 240, 072023.
- [19] Šedivý, D., Fialová, S., Jašíková, D. (2018). Flow of Newtonian and non-Newtonian fluid through pipe with flexible wall. In *AIP Conference Proceedings*, 2000, 020015.

Received March 18, 2020
Accepted June 15, 2020